Unprecedented scaling/fouling resistance of omniphobic polyvinylidene fluoride membrane with silica nanoparticle coated micropillars in direct contact membrane distillation

Zechun Xiao[1,2], Hong Guo[1], Hailong He[3], Yongjie Liu[1,3], Xuemei Li[1*], Yuebiao Zhang[3], Huabing Yin[4], Alexey V. Volkov [5], Tao He[1*]

[1]Shanghai Advanced Research Institute, Chinese Academy of Sciences, Shanghai 201210, China

[2]University of Chinese Academy of Sciences, Beijing 100049, China

[3]School of Physical Science and Technology, ShanghaiTech University, Shanghai 201210, China

[4]School of Engineering, University of Glasgow, Glasgow G12 8LT, UK

[5]Topchiev Institute of Petrochemical Synthesis RAS, Leninsky pr. 29, 119991, Moscow, Russia

*Corresponding authors: het@sari.ac.cn

Abstract

Recent development of omniphobic membranes shows promise in scaling/fouling mitigation in membrane distillation (MD), however, the fundamental understanding is still under dispute. In this paper, we report a novel omniphobic micropillared membrane coated by silica nanoparticles (SiNPs) (SiNPs-MP-PVDF) with dual-scale roughness prepared by a micromolding phase separation (μPS) and electrostatic attraction. This membrane was used as a model for analysis of scaling behavior by calcium sulfate ($CaSO_4$) scaling and fouling behavior by protein casein in comparison with commercial (C-PVDF) and micropillared (MP-PVDF) membranes. Unprecedented scaling/fouling resistance to $CaSO_4$ and casein was observed in direct contact membrane distillation (DCMD) for SiNPs-MP-PVDF membrane. Similar scaling and fouling occurred for commercial PVDF and micropillared PVDF membranes. The observation corresponds well to the wetting state of all membranes as SiNPs-MP-PVDF shows suspended wetting, but MP-PVDF shows pinned wetting. From a hydrodynamic view, the suspended wetting attributes a slippery surface which reduces the direct contact of foulants to solid membrane part and leads to significantly reduced fouling and scaling. However, a pinned (or metastable) wetting state leads to a stagnant interfacial layer that is prone to severe fouling and scaling. This work highlights that both scaling and fouling resistance are indeed of suspended wetting state and slippage origin.

Keywords: Omniphobic; Dual-scale roughness; Membrane distillation; Anti-fouling mechanism; slippery

1. Introduction

Water scarcity due to rising water demands and variable climate is threatening the global economy and sustainable development [1-3]. For many countries, industrial water pollution poses dramatic effects on the aquatic ecosystems [4]; however, if reclaimed, these streams would facilitate the sustainability of water resource. Conventional thermal process [5], reverse osmosis (RO) and electrodialysis (ED) have been applied up to a certain recovery ratio [6, 7]. However, the end high salinity fluids (~75000 mg/L) containing various concentrated foulants imposes constraints for these technologies on capital cost and maintenance [6, 8]. In recent years, membrane distillation (MD) as an emerging desalination technology has shown great promise in meeting such challenges [9-11] when integrated with available low-grade heat [12, 13]. MD is intrinsically more versatile than RO in treating complexed streams with a high salinity as MD is thermally driven with potentially ultrahigh rejection [14, 15].

However, MD membranes can suffer from severe fouling and scaling depending on the type of feed streams. Conventional hydrophobic microporous MD membranes are made from polymers such as polytetrafluroethylene (PTFE), polyvinylidene (PVDF) and polypropylene (PP) [16, 17]. When challenged by hypersaline wastewater of a complex composition (e.g., containing low surface tension contaminants and organic matter), membrane may incur fouling or pore wetting [18, 19]. Membrane fouling in MD refers to the deposition of undesired substance from bulk solution onto the membrane surface or plugging the pores [20]. Pore blockage by fouling reduces available pore area for evaporation, thereby causing severe concentration polarization and temperature polarization. This ultimately leads to a declined permeate flux and rejection [21, 22].

Fouling in MD generally falls into one of two categories: inorganic fouling (scaling) and organic fouling (protein, surfactant, etc.). The fouling process can be thermodynamically described by two patterns: 1) direct absorption or deposition of contaminant from bulk solution onto the membrane surface via intermolecular or surface forces and subsequent deposition; 2) Heterogeneous nucleation of fouling nuclei on the membrane surface followed by in-situ growth (especially for scaling). Direct absorption or deposition of foulants has been described successfully by the extended Derjaguin-Landau-Verwey-Overbeek (xDLVO) forces (van der Waals force, electrical double-layer force and the Lewis acid-based force) [23] and non-DLVO forces (steric force, hydration force, hydrophobic force, etc.) [24]. These forces can vary with the pH or ionic strength of intervening liquid medium and the chemical and physical properties (i.e., hydrophobicity or roughness, etc.) of the membrane surface.

In case of heterogeneous nucleation, the MD membrane surface facing the bulk solution provides the base of the nucleation site especially for the inorganic fouling (scaling), the probability of which is strongly dependent on its hydrophobicity and surface porosity according to Classical Nucleation Theory (CNT). However, the initial foulants/scalants tend to form the secondary fouling (e.g. deposited fouling also induces nucleation or growth) [25], leading to progressive wetting and performance reduction [26]. Established fouling mechanisms unraveled a thermodynamic understanding of fouling phenomena, and provided a guidance on alleviating or eliminating fouling/scaling by process parameter [27, 28] and membrane fabrication [17, 19, 29-33].

Inspired by nature, membranes with enhanced hydrophobicity (i.e. superhydrophobic surface) have been fabricated with ultralow surface energy and specific structures. These membranes were obtained by the combination of surface patterning and surface modification technologies. So far surface patterning methods include nano-micro fabrication by casting [34, 35] or imprinting [36] and

nanoparticles coating (SiO_2, ZnO and TiO_2) [13, 37-42], and surface modification involves the coating of the surface with low surface energy materials such as silanization [43, 44] and plasma fluorination [45-50]. Successes in fouling control and wetting mitigation in MD have been observed [17, 18, 20, 26].

Deployment of hydration layer [19, 51, 52] or engineered negative charge property [32, 45] by coating has demonstrated robust MD performances. Hydration layer formed by water-hydrophilic layer via hydrogen-bond blocks a direct attachment of foulants to the sub-hydrophobic membrane. Due to the negative surface charges in membrane surface, electrostatic repulsion to the matters in water which are also negatively charged contributes to fouling resistance. Studies in thermodynamic analysis indicate that increasing membrane hydrophobicity can deter the scaling formation as well as membrane wetting [21, 43, 53-55], however, the results sometimes are controversial as there are still scenarios in which superhydrophobicity has a negligible or even detrimental effect on fouling mitigation [16, 29, 30, 40, 56, 57]. Thereby, there still lacks definitive clarification on the anti-fouling mechanism for superhydrophobic or omniphobic membranes. We noticed that contemporary understanding of fouling in hydrophobic membranes is based on the thermodynamic and has been adopted from other membrane processes such as reverse osmosis, where a hydrophilic membrane is utilized.

Until very recently, we observed that a superhydrophobic membrane surface could behave in practice differently as previously assumed and described from a thermodynamic point [35, 58]. A novel concept of slippery surface was proposed as a hydrodynamic measure for scaling resistance [58]. Based on Navier's model, it is suggested that the flow velocity at the water-air-solid triple-phase interface for a hydrophobic membrane is above zero [58, 59]. This model has been adopted to explain the scaling resistance of superhydrophobic or omniphobic membrane in MD [35, 53, 58]. The enhancement of

flux by a slip flow was also expected from a theoretical approach [60]. Till present, the concept of slip is far from fully understood, but the correlation between slippage and local wetting state has been established: slippery property corresponds to a suspended wetting state and vice versa [58].

In this study, we further examine the scaling/fouling resistance of an omniphobic surface toward common organic foulant and scalant in order to verify the slippage effect on membrane fouling/scaling resistance. An omniphobic membrane was prepared by incorporating silica nanoparticles (SiNPs) to micro-pillared PVDF (MP-PVDF) membrane. The scaling by calcium sulfate and fouling by Casein were analyzed by comparison of DCMD flux and membrane autopsy. Wetting state was investigated, as well as a slippery surface was correlated to the fouling/scaling behavior. The new design and confirmation of correlation between slip - wetting state - fouling/scaling resistance highlight the importance of hydrodynamic contribution. The result from this study is expected to underpin a fundamental understanding of the anti-fouling mechanism of omniphobic membranes and may help design high-performance membranes to achieve a sustained MD performance for treating highly saline water streams with various foulants.

2. Materials and methods

2.1 Materials and chemicals

The silicon wafer mold with a pillar array (5 μm in diameter, 10 μm in height and period) was kindly provided by Suzhou Crystal Silicon Electronic and Technology Co. Ltd. Polydimethylsiloxane (PDMS) and the curing agent (Dow Corning, SYLGARD 184) were used to prepare the tailored casting substrate. PVDF (Solvay, Solef 1015), N, N-dimethylacetamide (DMAc, AR, Sinopharm) and diethylene glycol (DEG, AR, Sinopharm) were used for the fabrication of micropillared PVDF (MP-

PVDF) membrane. Tetraethyl orthosilicate (TEOS, AR, Sinopharm), ammonium hydroxide solution in water (AR, Sinopharm) and anhydrous ethanol (GR) were used for the preparation of silica nanoparticles. (Heptadecafluorotetrahydrodecyl)-triethoxysilane (17-FAS, 97%, Adamas), (3-Aminopropyl)-triethoxysilane (APTES, 99%, Sinopharm), and hexane (AR, General) were used for the surface modification of MP-PVDF membrane. Sodium chloride (NaCl, AR, Sigma-Aldrich), calcium chloride anhydrous ($CaCl_2$, AR, Sigma-Aldrich), sodium sulfate (Na_2SO_4, AR, Sigma-Aldrich), sodium chloride (NaCl, AR, Sinopharm), sodium bicarbonate ($NaHCO_3$, AR, Sinopharm) and Casein (Sinopharm) were used without further purification. Flat sheet commercial PVDF hydrophobic membrane (a nominal pore size of 0.22 μm and an average thickness of 125 μm) was purchased from Millipore, USA (abbreviated as C-PVDF, GVHP).

2.2 Fabrication of MP-PVDF membrane

A micromolding phase separation (μPS) method was utilized to fabricate a MP-PVDF membrane following a published procedure [58]: preparation of the PDMS casting substrate with a hexagonally arranged cylindrical hole array and membrane fabrication by non-solvent induced phase separation (NIPS). More details can be seen in Supplementary Information Method S1. A schematic diagram illustrating the fabrication process of MP-PVDF membrane is shown in Fig. 1.

2.3 Synthesis of silica nanoparticles

The silica nanoparticles (SiNPs) were prepared following a Stöber process [38]. Typically, a TEOS ethanol solution (by dissolving 10 mL TEOS in 40 mL anhydrous ethanol) was added into a mixture of water (21.8 mL), ammonium hydroxide (10 mL) and anhydrous ethanol (16.3 mL) under vigorous stirring (600 rpm) until a silvery color solution was obtained. Afterwards, the solution was stirred at

400 rpm for 5 h. Finally, the resultant white, turbid suspension was rinsed with ethanol for 4 times and dried at ~50 °C for 24 h. The aqueous SiNPs solution was prepared by adding 0.1 wt.% SiNPs in anhydrous ethanol and bath sonicated for 30 min to minimize particle aggregation.

2.4 Surface modification of MP-PVDF membrane

A micropillared PVDF (MP-PVDF) membrane was treated with O_2 plasma (IoN40, PVA Tepla Co. Ltd) at 50 w for one min [61] and then placed immediately into 1% v/v APTES in anhydrous ethanol at 40 °C for 2 h [38]. Subsequently, the MP-PVDF membrane was immersed in an aqueous SiNPs suspension for 1 h allowing negatively charged [45] SiNPs to absorb to the positively charged membrane surface based on electrostatic interaction. Afterwards, the membrane was immersed in 1% v/v 17-FAS solution in hexane at 65 °C for 48 h, in which a hydrolysis-condensation reaction generates a surface with ultralow surface energy, followed by thorough rising with hexane and then subjecting to heat treatment at 100 °C for 1 h. The resultant membrane was denoted as SiNPs-MP-PVDF membrane. A schematic diagram illustrating the procedure for the fabrication of SiNPs-PVDF membrane is shown in the Fig. 1.

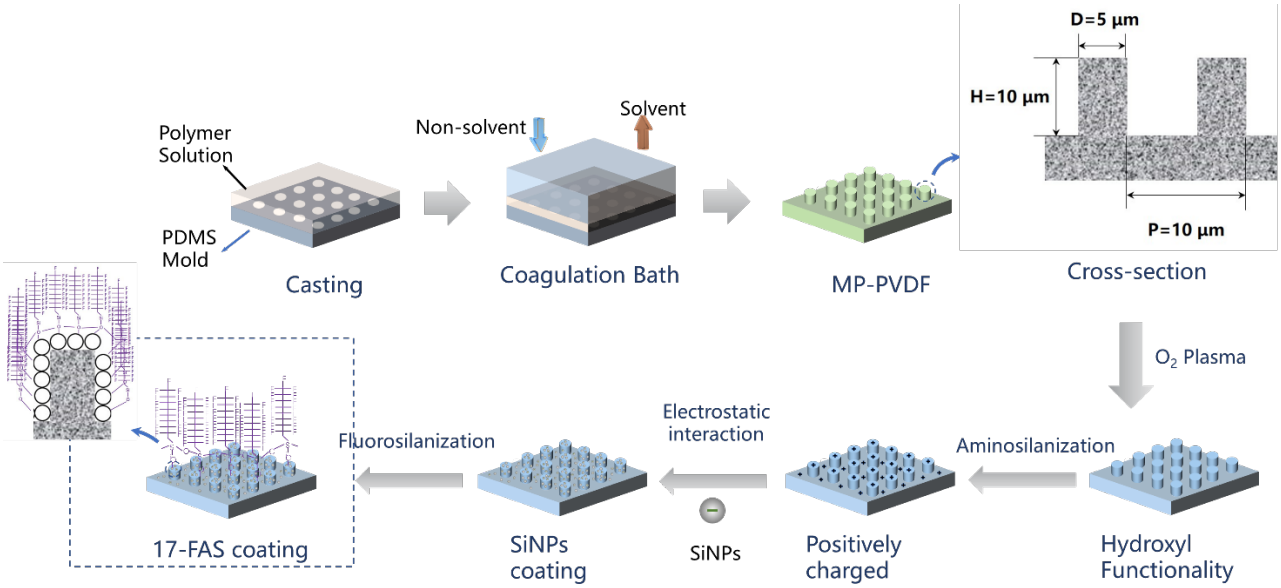

Fig. 1 Schematic for fabricating MP-PVDF and SiNPs-MP-PVDF membrane. (Top) Preparation of MP-PVDF membrane by a micromolding phase separation (μPS) method. The MP-PVDF membrane has pillars with the dimension of ~5 μm (diameter), ~10 μm (height) and ~10 μm (Period); (bottom) Omniphobic surface modification of MP-PVDF membrane to fabricate SiNPs-MP-PVDF membrane.

2.5 Membrane characterization

Scanning electron microscopy (HITACH TM-1000 and FEI Nova Nano SEM 450) was utilized to characterize the surface morphology of each membrane before and after MD test.

The surface wettability of the membranes was assessed using a CA goniometer (Maist Drop Meter A-100P) equipped with a high-speed CCD camera. Static contact angles of DI water (γ = 72.8 mN/m), 4 % SDS (γ = 34.2 mN/m), and hexadecane (98%, Sinopharm, γ = 27.5 mN/m) were evaluated via the sessile drop method (a liquid droplet of 5 μL). To measure the sliding angle, a water droplet of 5 μL was placed on a horizontal membrane surface fixed on the testing stage. The stage was then tilted slowly to allow the droplet to slide off the surface, which was recorded by the high-speed CCD camera. The sliding angle was determined as the tilting angle of the stage at which the water droplet starts to slide.

X-ray photoelectron spectroscopy (XPS) was employed to investigate the elemental composition of the membranes using an ESCALAB 250Xi (Thermo). A monochromatic Al Kα line (1486.6 eV) was used for XPS. Mean pore size of the membranes was measured by Capillary Flow Porometry (Porolux 1000) via a wet/dry flow method. The durability of SiNPs and 17-FAS coating was assessed by subjecting SiNPs-MP-PVDF membrane to bath sonication and subsequent measurement of static contact angle and SEM analysis.

178 **2.6 MD performance**

179 A lab-scale direct contact membrane distillation (DCMD) unit (Supplementary Information Fig.
180 S1) was used to evaluate the desalination performance and fouling behavior of the membranes. Two
181 different feed solutions were employed: 1) $CaSO_4$ solution (initial volume of 1.2 L) was prepared by
182 mixing 14.7 mM $CaCl_2$ and 14.7 mM Na_2SO_4 solutions at a certain ratio. The feed and permeate
183 temperatures were 70 and 20 ^oC, respectively (14.7 mM $CaSO_4$ was supersaturated at 70 ^oC and
184 saturation index (SI) = 1.2 [58]); 2) A synthetic Casein solution was prepared by dissolving 240 mg/L
185 Casein, 111 mg/L $CaCl_2$, 400 mg/L $NaHCO_3$ and 1170 mg/L NaCl in DI water (initial volume of 1.0
186 L) based on our previous work [19]. The solution pH was adjusted to 7.0 by adding small quantities of
187 0.1 M NaOH or 0.1 M HCl as needed before MD test. The feed and permeate temperature were 60 and
188 20 ^oC, respectively. The same flow rate of the feed and permeate was maintained at 600 mL/min. The
189 water vapor flux (J, $kg/m^2 \cdot h$) across the membrane was determined by measuring the increase in the
190 permeate weight. Electric conductivity of the permeate stream was monitored by a conductivity sensor
191 (EC-4300RS, supplied by SUNTXE Instrument Ltd.) to facilitate the detection of the membrane
192 wetting.

193 **3. Results and discussion**

194 **3.1 Characterization of membranes**

195 SEM images (Fig. 2a) displayed the surface morphologies of the C-PVDF, MP-PVDF and SiNPs-
196 MP-PVDF membranes. Porous surfaces were observed in C-PVDF and MP-PVDF membranes. The
197 MP-PVDF membrane has porous pillars with the dimension of ~5 μm (diameter), ~10 μm (height) and
198 ~10 μm (Period). The SEM image of SiNPs-MP-PVDF membrane showed that silica nanoparticles

199 covered top and the side of the pillar surface as well as the bottom surface below the pillars
200 demonstrating a hierarchical morphology where nanoparticle covered micropillar arrays. Size
201 distribution of SiNPs was shown in Supplementary Information Fig. S2. The particle size of SiNPs
202 ranges from ~ 610 nm to 840 nm. After SiNPs and 17-FAS coating, the mean flow pore size (~ 105
203 nm) of SiNPs-MP-PVDF membrane was slightly reduced as compared to the pristine MP-PVDF
204 membrane (~ 120 nm) due to the close-packed particle layer (Table 1). In 2008, Li and coworkers [62]
205 published a similar structure combining micropillar arrays with silica nanoparticles. It was shown that
206 the combined structure changes the surface wettability from metastable superhydrophobicity to
207 ultraphobicity. However, the particles were only deposited at pillar tips. Here we have shown that
208 particles covered the tip, side wall and the bottom surface, demonstrating a true dual-scale roughness,
209 which may further enhance the water repellence as will be discussed in further paragraphs.

210 Fig. 2c gives the XPS spectra of the C-PVDF, MP-PVDF and SiNPs-MP-PVDF membranes. In
211 the spectrum of C-PVDF and pristine MP-PVDF membranes, two prominent peaks are ascribed to F1s
212 and C1s lines. The nearly identical survey scan spectra are not surprising since both membranes are of
213 the same chemical nature (similar element composition shown in Table 1). An insignificant amount of
214 Si (0.38 % for C-PVDF and 0.51 % for MP-PVDF) was most probably caused by the contamination
215 of sample from air or glassware during sample preparation. For the SiNPs-MP-PVDF membrane,
216 additional peaks for Si 2s, Si 2p and O 1s and significant content of O (6.23 %) and Si (3.31) (Table 1)
217 were observed. Increase of F content from MP-PVDF to SiNPs-MP-PVDF membrane (51.56 % to
218 52.96 %) indicated the successful fluorination with 17-FAS.

219 Static contact angles of the membranes toward fluids of different surface tensions are presented in
220 Fig. 2b. A water contact angle of 155 ^{o} was observed on the MP-PVDF membrane, much higher than

that of the C-PVDF (130 °) owing to the extra area fraction of air provided by the porous pillars. However, both of C-PVDF and MP-PVDF failed to resist a 4 % SDS solution and hexadecane (photograph in the Fig. 2b). The contact angle of the C-PVDF (63 °) and MP-PVDF (84 °) toward the 4 % SDS was dramatically lower than that to water. Instant wicking of hexadecane hints that they are lipophilic toward the low surface tension liquid (γ = 27.5 mN/m). Notably, the SiNPs-MP-PVDF membranes exhibited robust omniphobicity with a water contact angle of 175° and a hexadecane contact angle of 151°. This omniphobicity is attributed to the hierarchical structure (a dual-scale roughness composing of spherical SiNPs and cylindrical micropillars) and the low surface energy of 17-FAS coating layer.

A relatively low sliding angle, ~ 15.8 °, for the MP-PVDF membrane was observed (Table 1), whereas water droplet sticks to the C-PVDF membrane (sliding angle > 90 °). SiNPs-MP-PVDF membrane exhibited an ultralow water sliding angle of ~ 3.5 °, which was attributed to the dual scale roughness and surface coating [63]. Using the surface wettability data, the surface energy was deduced. The C-PVDF membrane represents the highest surface energy of 66 mJ/m^2, whereas the SiNPs-MP-PVDF membrane shows the lowest energy of 0.24 mJ/m^2. Notably, since the calculation of surface energy employed the apparent contact angle of the polar and non-polar on membrane surfaces not a perfectly smooth surface, surface energy of SiNPs-MP-PVDF membrane is much lower than the lowest surface energy that could be achieved (~ 7 mJ/m^2) according to the literature [64] due to the effect of dual-scale roughness.

The durability of SiNPs and 17-FAS coating was examined by sonication for 30 min. No apparent difference could be seen in surface morphology of SiNPs-MP-PVDF membranes (Fig. S3a). In addition, wetting properties against three fluids exhibited only a slightly reduction as compared to the

initial one (Supplementary Information Fig. S3b), confirming the robustness of surface modification with the SiNPs and 17-FAS coating.

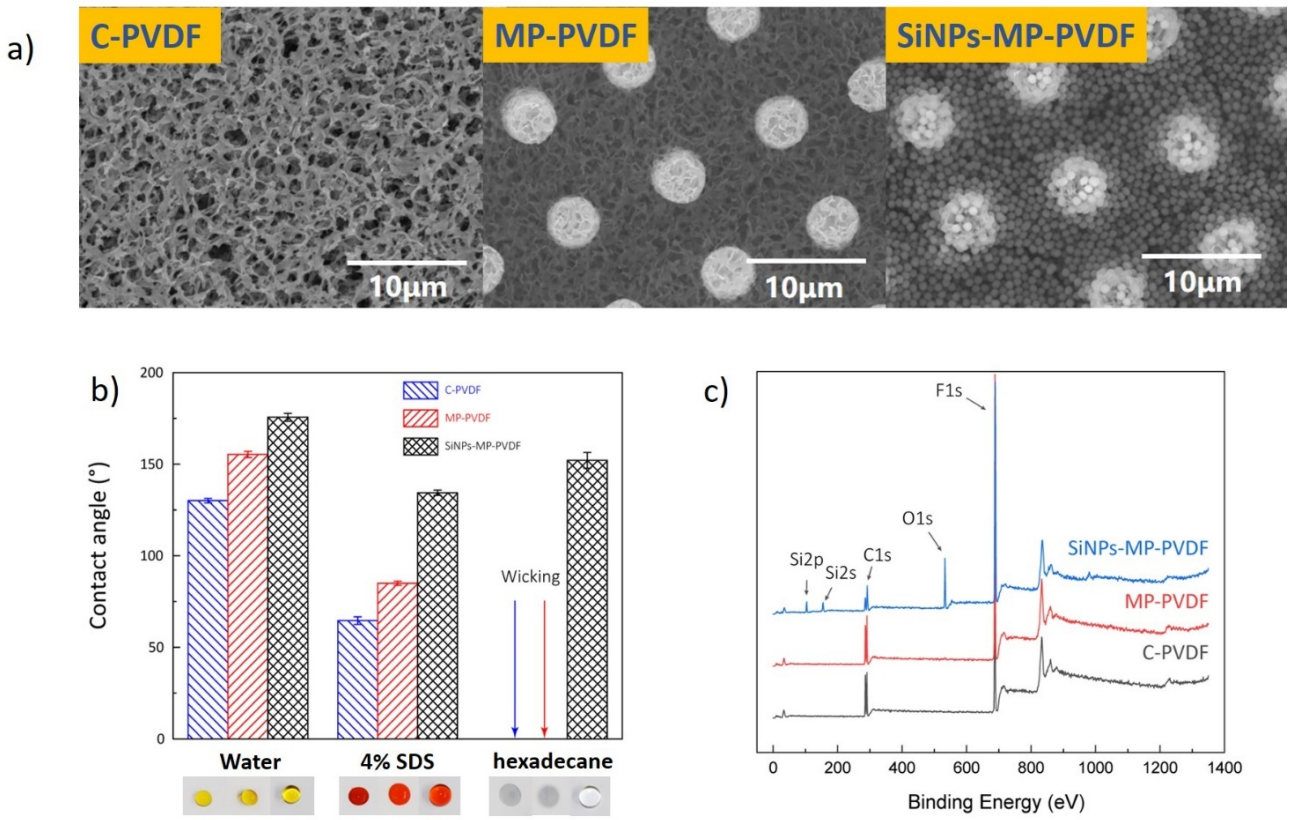

Fig. 2 (a) SEM images of C-PVDF, MP-PVDF and SiNPs-MP-PVDF membrane surfaces. The mean size of silica nanoparticles is ~640 nm. (b) Apparent contact angle of liquids with different surface tensions on the C-PVDF, MP-PVDF and SiNPs-MP-PVDF. Water (γ = 72.8 mN/m), 4 % SDS (γ = 34.2 mN/m) and hexadecane (γ = 27.5 mN/m) [38]. Error bars represent standard deviation from five independent measurements. Images of the wetting behavior for both membranes are shown underneath the bar graph. (c) X-ray photoelectron spectroscopy (XPS) survey scan spectra of the C-PVDF, MP-PVDF and SiNPs-MP-PVDF membranes.

256 Table 1 Characteristics of the C-PVDF, MP-PVDF and SiNPs-MP-PVDF membranes

Membrane		C-PVDF	MP-PVDF	SiNPs-MP-PVDF
Thickness/μm		132 ± 3	263 ± 2	268 ± 3
Mean pore size/μm		0.235 ± 0.013	0.120 ± 0.005	0.105 ± 0.027
Water contact angle/^{o}		130.1 ± 1.2	155.3 ± 1.7	175.6 ± 2.1
Water sliding angle/^{o}		> 90	15.8 ± 3.3	3.5 ± 2.1
Surface energy [a] /mJ/m^2		65.8 ± 3.2	43.9 ± 1.4	0.24 ± 0.1
LEP_W [b] /MPa		0.237 ± 0.003	0.239 ± 0.002	0.307 ± 0.012
Element composition	C/%	47.16	47.39	37.49
	F/%	51.94	51.56	52.96
	O/%	0.52	0.53	6.23
	Si/%	0.38	0.51	3.31

257 [a] Supplementary Information Method S2 for determination of surface energy.

258 [b] Liquid entry pressure of DI water.

259 **3.2 DCMD performance**

260 **3.2.1 Scaling behavior**

261 The scaling behavior of the C-PVDF, MP-PVDF and SiNPs-MP-PVDF membranes was compared
262 using a supersaturated $CaSO_4$ (14.7 mM in 70 ^{o}C [65]) in a DCMD concentration process as illustrated
263 in Fig. 3a. To make a reasonable comparison between the three membranes, a flux decline at 50% was
264 selected as the check point. Saturation or supersaturation is a thermodynamic factor for nucleation and
265 growth of crystals [66]. Further, a certain induction time is required prior to the formation of detectable

crystalline phase. In the induction period, the solution remains saturated or supersaturated in a metastable equilibrium without any occurrence of crystallization [66].

For the C-PVDF and pristine MP-PVDF membranes, a stable MD flux was observed during the extended induction time until a concentration factor (CF) of 1.6 and 1.7, respectively; thereafter MD flux declined for both membranes. The MP-PVDF membrane showed slightly better scaling resistance. Because initial $CaSO_4$ solution was supersaturated at 70 ^oC, the stable flux as shown in Fig. 3a indicates that both membranes could tolerate supersaturated solution to a certain extent [66, 67]. Very different MD performance of SiNPs-MP-PVDF was observed (green triangle in Fig. 3a): no flux decline was observed up to a concentration factor of 2.1 until end of the experiment due to limit in the feed tank volume. SEM images of the membranes after the concentration experiments (Fig. 3b, 3c and 3d) showed that both C-PVDF and MP-PVDF membranes were fully covered by $CaSO_4$ crystals, whereas the SiNPs-MP-PVDF membrane surface remained clean. This is a direct experimental evidence of super scaling resistance of the SiNPs-MP-PVDF membrane.

Classical nucleation theory suggests that membrane with greater hydrophobicity presents a higher energetic barrier to heterogeneous nucleation [66]. From the coverage of crystals and flux patterns, it indeed showed that the hydrophobicity is related to the performance of the membranes. For the SiNP-MP-PVDF membrane, no fouling was observed, which is ascribed to the ultrahigh water repellency. Nevertheless, the hydrophobicity alone does not appear to be the only deterministic factor for fouling resistance as controversies over the relationship between superhydrophobicity and anti-fouling effects has been reported [16, 29, 30, 40, 56, 57].

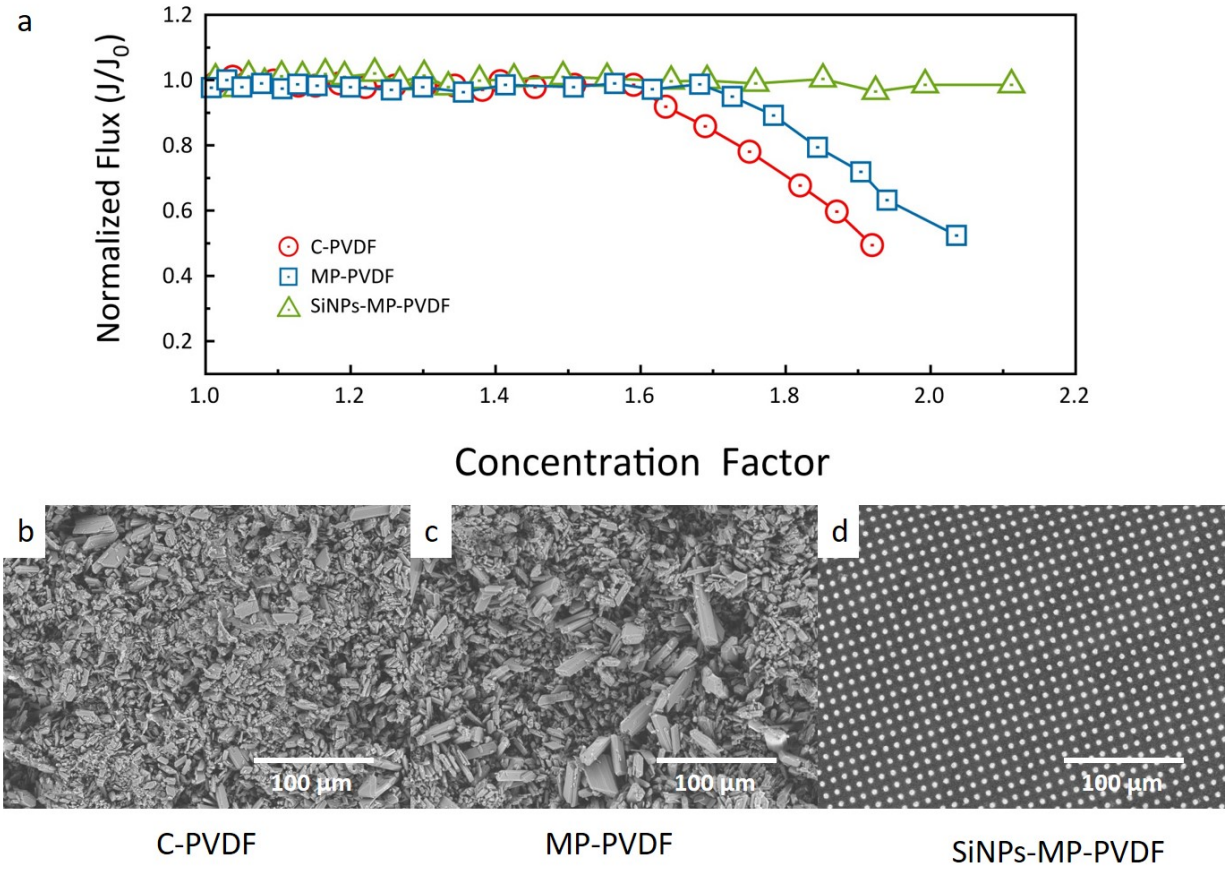

286

287 Fig. 3 (a) DCMD performance of C-PVDF, MP-PVDF and SiNPs-MP-PVDF membranes. Normalized
288 water vapor flux (J/J_0) as a function of concentration factor (CF) (ratio of the feed salt concentration
289 in process to the initial concentration). Feed: 14.7 mM $CaSO_4$. Feed/Permeate temperature: 70 °C/20
290 °C. Initial flux J_0 of C-PVDF, MP-PVDF and SiNPs-MP-PVDF was 35.1 kg/m^2·h, 31.5 kg/m^2·h [58]
291 and 24.3 kg/m^2·h, respectively. SEM images of (b) C-PVDF, (c) MP-PVDF and (d) SiNPs-MP-PVDF
292 membranes after the DCMD experiments.

293 **3.2.2 Fouling by Casein**

294 To examine the membrane fouling against organic foulant, a synthetic 240 mg/L Casein feed
295 solution was used at a relatively low salinity (i.e., ~ 1600 mg/L). Fig. 4a illustrates the MD performance
296 of the three membranes. Significant flux declines of C-PVDF and MP-PVDF were observed in Fig. 4a
297 (red circle and blue square) and aggravated fouling layer deposited on the C-PVDF and MP-PVDF

298 membrane surface after MD tests (Fig. 4b and 4c). Tracked permeate conductivity showed that no
299 obvious salt leakage occurred in all experiments. This suggested that the change in flux was solely
300 attributed to deposition of foulants on the membrane surface or pore blocking. However, the SiNPs-
301 MP-PVDF membrane is exceptionally resistant to fouling by Casein as indicated by stable flux (green
302 triangle in Fig. 4a) and the membrane surface remained free of any traces of foulants (Fig. 4d). Since
303 Casein is intrinsically hydrophobic due to a high number of proline residue, there may exist a strong
304 tendency to deposit on a hydrophobic surface via hydrophobic forces [24, 68]. Furthermore, the iso-
305 electric point of Casein is 4.6 [68], thus Casein is negatively charged at pH 7. Calcium (111 mg/L) and
306 sodium (1170 mg/L) ions could form ionic complexes with two carboxyl groups in Casein, and this
307 could aggregate membrane fouling [27, 69]. For C-PVDF and MP-PVDF membrane, the flux reduction
308 was ascribed to the pore blockage by fouling layer (Fig. 4b and 4c), where similar fouling layer
309 uniformly deposited on both membrane surfaces. We noticed that the pictures were taken from the
310 center part of the membranes, where fouling was mild; at the membrane edge, fouling was significantly
311 more severe as in Supplementary Information Fig. S4. This difference was mainly due to reduced flow
312 velocity close to module (Fig. S4).

313 Boo et al [29] claimed that hydrophobic interaction between hydrophobic foulant and membrane
314 surface increases with decreasing membrane surface energy. This means that SiNPs-MP-PVDF
315 membrane would be more susceptible to Casein fouling than commercial membrane because of its
316 lower surface energy (0.24 mJ/m^2). However, excellent fouling resistance of SiNPs-MP-PVDF
317 membrane revealed that contrary to prior accepted theory, surface energy is not a deterministic factor
318 for fouling. With a special interest in the surface patterning, Xie et al [36] demonstrated that a surface-
319 patterned superhydrophobic polytetrafluoroethylene (PTFE) membrane by nanoimprint strongly

resisted fouling by bovine serum albumin (BSA, a hydrophobic protein). However, we found that a superhydrophobic MP-PVDF membrane with micropattern did not show obvious improvement in the fouling resistance to proteins. Both of theories from Boo et al [29] and Xie et al [36] had an origin of thermodynamic basis, in which the interaction between foulants and the membrane surface is guaranteed with sufficient time. If this assumption is not absolutely correct, probably, other factors might play more important role in determining the fouling behavior of superhydrophobic and omniphobic membranes.

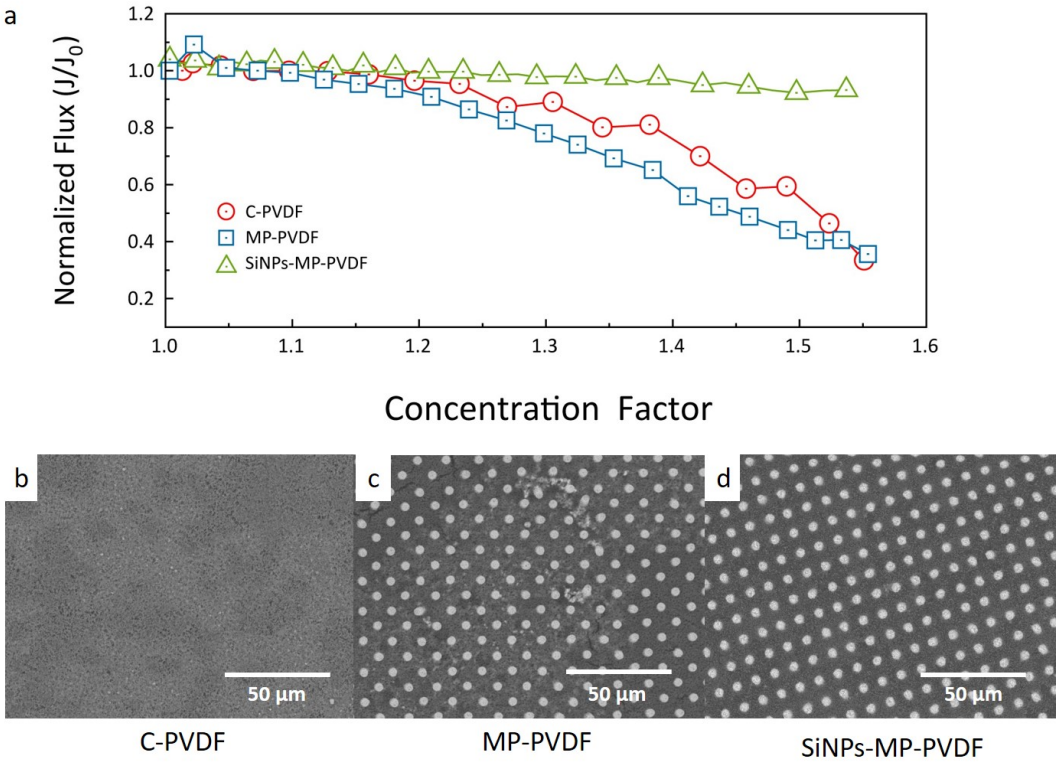

Fig. 4 a: MD performance of C-PVDF, MP-PVDF and SiNPs-MP-PVDF membranes. Normalized water vapor flux (J/J_0) as a function of concentration factor (CF). Feed: Synthetic Casein solution including 240 mg/L Casein, 111 mg/L $CaCl_2$, 400 mg/L $NaHCO_3$ and 1100 mg/L NaCl. Feed/Permeate temperature: 60 ºC/20 ºC. Initial flux J_0 of C-PVDF, MP-PVDF and SiNPs-MP-PVDF was 24.3

332 kg/m^2·h, 23.6 kg/m^2·h and 18.1 kg/m^2·h, respectively. SEM images were taken from the center section
333 of (b) C-PVDF, (c) MP-PVDF and (d) SiNPs-MP-PVDF membranes after the DCMD experiments.
334 Refer to Fig. S4 in the Supplementary Information for details.
335

336 **3.3 Mechanisms of fouling mitigation with SiNPs-MP-PVDF**

337 In our previous work, we have demonstrated a correlation between scaling resistance and wetting
338 state of membranes by theoretical analysis and measurement of the slip length [58]. The suspended
339 wetting state with a positive slip length (i.e. MP-PVDF treated by CF_4 plasma) yields a slippage at the
340 local liquid-air-membrane interface, thus being scaling resistant; whereas pinned state with a negative
341 slip length (i.e. C-PVDF and MP-PVDF) readily incurs scaling by crystal deposition or in-situ
342 nucleation. Slippage upon suspended wetting results from gas trapped between nano- or microstructure
343 [70]. A large fraction of air for a suspended state leads to a low liquid-solid contact area, and high flow
344 velocity by slippage at the air-liquid-solid interface, which means short residence time of liquid on the
345 solid section of the membrane surface. However, at a pinning state, a stagnant liquid layer remains
346 which is very similar to a hydrophilic membrane surface, thus serves as a site for scaling. There seems
347 a strong correlation between wetting state, slip and scaling resistance. Therefore, evaluation of the
348 wetting state is crucial.

349 Similar to our previous results, the pinned wetting state of C-PVDF (sliding angle > 90 ^{o}) led to a
350 static liquid layer at the interface. For MP-PVDF membrane, theoretical analysis by Grewal et al
351 suggested that pillars on MP-PVDF membrane also lead to a pinned wetting state (Fig. 5a) [58, 71].
352 Wetting state of MP-PVDF membrane was determined by wetting state factor ζ, which can be
353 calculated based on the structure parameter and advancing angle of MP-PVDF membrane (~157 ^{o} [58]).

354 A suspended state to transition state occurs at $\zeta < 0.5$, whereas a transition state to pinned state occurs
355 at $0.75 > \zeta > 0.5$ and a pinned state is observed at $\zeta > 0.75$ (Fig. 5a) [58, 71]. Details of calculation are
356 shown in Supplementary Information Method S3. Zero local flow velocity at the interface provides a
357 long residence time for nucleation and growth of $CaSO_4$ as well as the interaction between membrane
358 materials and the foulants. As a result of similar hydrodynamic condition, very similar fouling behavior
359 for both scaling of $CaSO_4$ and Casein was observed in DCMD for both membranes (Fig. 3a and Fig.
360 4a).

361 The wetting state of SiNPs-MP-PVDF membrane could be determined by the theoretical analysis
362 by Wu et al [72, 73]. For a surface with dual-scale roughness, the wetting states are related to the
363 apparent contact angle, the magnitude of primary and the secondary roughness. Fig. 5b shows the result
364 of theoretical analysis, in which wetting state is determined by apparent contact angle at a
365 period/diameter of 2 ($P/D = 10/5 = 2$). Suspended wetting state occurs at apparent contact angle > 146
366 ^{o}, whereas a transition state occurs between 137 ^{o} and 146 ^{o}, and a pinned state occurs at apparent
367 contact angle < 137 ^{o} (Supplementary Method S4). Omniphobic SiNPs-MP-PVDF membrane is
368 featured with ultrahigh contact angle (175 ^{o}), indicating a suspended wetting (Fig. 5b).
369
370

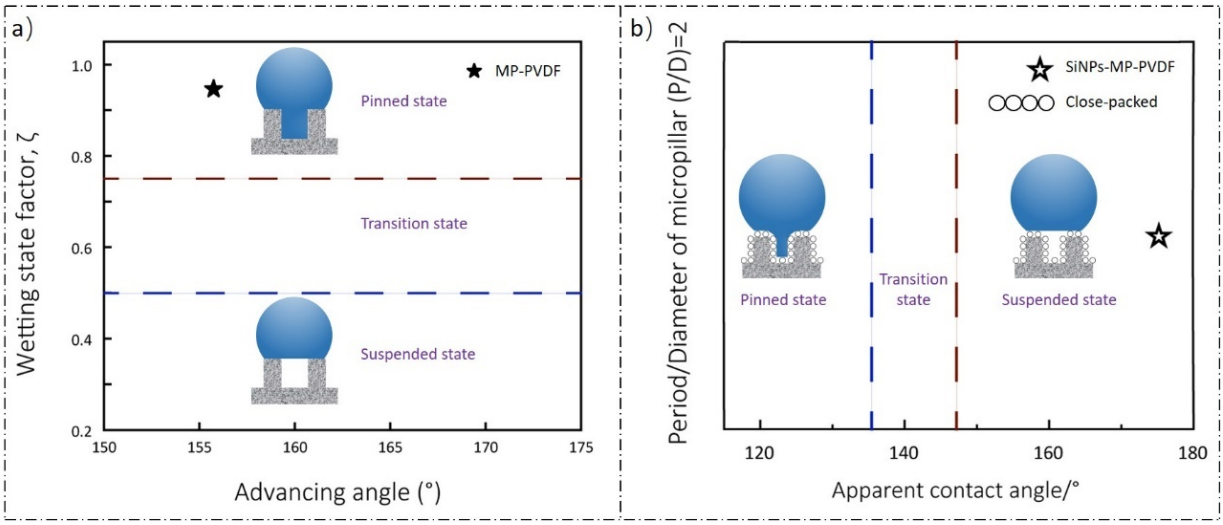

Fig. 5 (a) Map of the wetting state factor based on work by Grewal et al [58, 71] for micropillared membrane: A suspended state to transition state occurs at $\zeta < 0.5$, whereas a transition state to pinned state occurs at $0.75 > \zeta > 0.5$ and a pinned state is observed at $\zeta > 0.75$; (b) Map of the wetting states based on work by Wu et al [72, 73] for dual-scale roughness surface at P/D of 2: suspended wetting occurs at apparent contact angle > 146 °, whereas a transition occurs between 137 ° - 146 °, and pinned state occurs at apparent contact angle < 137 °. Insert is a schematic of a close-packed array. The transition state from the suspended to the pinned states on surfaces with dual-scale roughness is defined as a metastable state with partial liquid intrusion due to Laplace pressure [74].

The suspended wetting for SiNPs-MP-PVDF represents a typical "lift up" effect (Fig. 5b). This configuration effectively minimizes the liquid-solid contact area and reduces the probability for the interaction between foulant and membrane surface. It also enlarges the evaporation area to alleviate dramatic flux decline by the SiNPs coating. Further, from a hydrodynamic point, the suspended state substantially generates a slippery surface, reducing the drag to fluid due to non-static water layer at the interface. The interfacial flow corresponds to a shorter residence time for nucleation of $CaSO_4$ crystal and interaction between foulants and solid polymeric part in membrane. The flow also generates a

388 shear force due to slippage is also beneficial for preventing the attachment of foulants in the feed
389 stream.

390 In addition, the robustness of omniphobic SiNPs-MP-PVDF membrane was confirmed by
391 measuring the contact angle after scaling ($CaSO_4$) and fouling (Casein) tests. The contact angle
392 reduced from original 175.6 ± 2.1° to 164.6 ± 1.9° for scaling test and 166.6 ± 1.3 ° after Casein test.
393 Based on the model (Fig. 5b), the SiNPs-MP-PVDF membrane after MD tests remained suspended
394 wetting state. Slight reduction in water contact angle was caused by the feed residual attached to the
395 surface. The results demonstrated that wetting state of SiNPs-MP-PVDF membrane during DCMD
396 trials was a suspended wetting, which contributed to the scaling/fouling resistance. As a summary, by
397 combining the micropillars and nanoparticles, a dual-scale roughness creates a low energy surface with
398 slippage; this extra hydrodynamic property contributes to superior scaling and fouling resistance in
399 MD.

400 **4. Conclusion**

401 In this work, an omniphobic SiNPs-MP-PVDF membrane with dual-scale roughness was prepared
402 via a micromolding phase separation (μPS) incorporating silica nanoparticles (SiNPs). The scaling
403 resistance to $CaSO_4$ and fouling resistance to Casein were investigated in DCMD in comparison with
404 commercial PVDF (C-PVDF) and micropillared PVDF (MP-PVDF) membranes. Similar scaling/
405 fouling performance was found for C-PVDF and MP-PVDF, but stable MD performance was found
406 for SiNPs-MP-PVDF for both scaling and protein fouling. This superior fouling resistance of
407 omniphobic SiNPs-MP-PVDF membrane was attributed to the suspended wetting state as determined
408 using the model for dual-scale roughness surface. A suspended wetting corresponds to an interfacial
409 slippage which in turn promotes shear force for preventing deposition of foulants as well reduced the

probability for nucleation and fouling. Our previous work demonstrated that a slippage superhydrophobic membrane is scaling resistant. Present work showed that omniphobic membrane is simultaneously scaling/fouling resistant. Both results provided solid proof that scaling/fouling resistance of hydrophobic surface is probably not of a thermodynamic, but a hydrodynamic origin. However, a final understanding requires a systematic research on the contribution of each factor (i.e. micro pillar, silica nanoparticles and 17-FAS coating) to fouling and scaling in DCMD. Under the framework of wetting state, slip and scaling/fouling resistance, we expect a final engineering design based on understanding of the contribution of above factors.

5. Acknowledgements

The research was partially supported by National Natural Science Foundation of China (No. 21978315, 21676290, 51861145313), Newton Advanced Fellowship (Grant No. NA170113). We also thank the frame work research consortium for partially financial support (RFBR No. 18-58-80031, NSFC No. 51861145313, DST IPN/7864, NRT No.116020, CNPq/BRICS-STI-2-442229/2017-8).

6. Reference

[1] C. Vörösmarty, P. Mcintyre, M. Gessner, D. Dudgeon, A. Prusevich, P. Green, S. Glidden, S. Bunn, C. Sullivan, C. Liermann, Global threats to human water security and river biodiversity, Nature, 467 (2010) 555-561.

[2] S.B. Grant, J.-D. Saphores, D.L. Feldman, A.J. Hamilton, T.D. Fletcher, P.L.M. Cook, M. Stewardson, B.F. Sanders, L.A. Levin, R.F. Ambrose, Taking the "Waste" Out of "Wastewater" for Human Water Security and Ecosystem Sustainability, Science, 337 (2012) 681-686.

[3] Hoekstra, A. Y., Water scarcity challenges to business, Nature Climate Change, 4 (2014) 318-320.

[4] Schwarzenbach, Egli, Hofstetter, V. Gunten, Wehrli, Global Water Pollution and Human Health, Social Science Electronic Publishing, 35 (2010).

[5] N. Ghaffour, T.M. Missimer, G.L. Amy, Technical review and evaluation of the economics of water desalination: current and future challenges for better water supply sustainability, Desalination, 309 (2013) 197-207.

[6] T. Tong, M. Elimelech, The global rise of zero liquid discharge for wastewater management: drivers, technologies, and future directions, Environmental science & technology, 50 (2016) 6846-6855.

[7] M. Elimelech, W.A. Phillip, The Future of Seawater Desalination: Energy, Technology, and the Environment, Science, 333 (2011) 712-717.

[8] A. Al-Karaghouli, L.L. Kazmerski, Energy consumption and water production cost of conventional and renewable-energy-powered desalination processes, Renewable and Sustainable Energy Reviews, 24 (2013) 343-356.
[9] A. Alkhudhiri, N. Darwish, N. Hilal, Membrane distillation: A comprehensive review, Desalination, 287 (2012) 2-18.
[10] A.M. Alklaibi, N. Lior, Membrane-distillation desalination: Status and potential, Desalination, 171 (2005) 111-131.
[11] E. Curcio, E. Drioli, Membrane Distillation and Related Operations—A Review, Separation & Purification Reviews, 34 (2005) 35-86.
[12] A. Deshmukh, C. Boo, V. Karanikola, S. Lin, A.P. Straub, T. Tong, D.M. Warsinger, M. Elimelech, Membrane distillation at the water-energy nexus: limits, opportunities, and challenges, Energy & Environmental Science, 11 (2018) 1177-1196.
[13] S. Lin, S. Nejati, C. Boo, Y. Hu, C.O. Osuji, M. Elimelech, Omniphobic membrane for robust membrane distillation, Environmental Science & Technology Letters, 1 (2014) 443-447.
[14] H.C. Duong, A.R. Chivas, B. Nelemans, M. Duke, S. Gray, T.Y. Cath, L.D. Nghiem, Treatment of RO brine from CSG produced water by spiral-wound air gap membrane distillation—a pilot study, Desalination, 366 (2015) 121-129.
[15] X.-M. Li, B. Zhao, Z. Wang, M. Xie, J. Song, L.D. Nghiem, T. He, C. Yang, C. Li, G. Chen, Water reclamation from shale gas drilling flow-back fluid using a novel forward osmosis–vacuum membrane distillation hybrid system, Water Science and Technology, 69 (2014) 1036-1044.
[16] Z. Wang, S. Lin, Membrane fouling and wetting in membrane distillation and their mitigation by novel membranes with special wettability, Water research, 112 (2017) 38-47.
[17] K.J. Lu, Y. Chen, T.-S. Chung, Design of omniphobic interfaces for membrane distillation–a review, Water research, (2019).
[18] L.D. Tijing, Y.C. Woo, J.-S. Choi, S. Lee, S.-H. Kim, H.K. Shon, Fouling and its control in membrane distillation—A review, Journal of Membrane Science, 475 (2015) 215-244.
[19] J. Wang, H. He, M. Wang, Z. Xiao, Y. Chen, Y. Wang, J. Song, X.-M. Li, Y. Zhang, T. He, 3-[[3-(Triethoxysilyl)-propyl] amino] propane-1-sulfonic acid zwitterion grafted polyvinylidene fluoride antifouling membranes for concentrating greywater in direct contact membrane distillation, Desalination, 455 (2019) 71-78.
[20] D.M. Warsinger, J. Swaminathan, E. Guillen-Burrieza, H.A. Arafat, Scaling and fouling in membrane distillation for desalination applications: a review, Desalination, 356 (2015) 294-313.
[21] T. Tong, A.F. Wallace, S. Zhao, Z. Wang, Mineral scaling in membrane desalination: Mechanisms, mitigation strategies, and feasibility of scaling-resistant membranes, Journal of Membrane Science, 579 (2019) 52-69.
[22] T. Zou, X. Dong, G. Kang, M. Zhou, M. Li, Y. Cao, Fouling behavior and scaling mitigation strategy of CaSO 4 in submerged vacuum membrane distillation, Desalination, 425 (2018) 86-93.
[23] C. Van Oss, Acid—base interfacial interactions in aqueous media, Colloids and Surfaces A: Physicochemical and Engineering Aspects, 78 (1993) 1-49.
[24] J.N. Israelachvili, Intermolecular and surface forces, Academic press, 2015.
[25] X. Jiang, D. Lu, W. Xiao, G. Li, R. Zhao, X. Li, G. He, X. Ruan, Interface‐based crystal particle autoselection via membrane crystallization: From scaling to process control, AIChE Journal, 65 (2019) 723-733.
[26] M. Rezaei, D.M. Warsinger, M.C. Duke, T. Matsuura, W.M. Samhaber, Wetting phenomena in membrane distillation: mechanisms, reversal, and prevention, Water research, 139 (2018) 329-352.
[27] D. Hou, D. Lin, C. Zhao, J. Wang, C. Fu, Control of protein (BSA) fouling by ultrasonic irradiation during membrane distillation process, Separation and Purification Technology, 175 (2017) 287-297.
[28] Y. Ye, S. Yu, L.a. Hou, B. Liu, Q. Xia, G. Liu, P. Li, Microbubble aeration enhances performance of vacuum membrane distillation desalination by alleviating membrane scaling, Water research, 149 (2019) 588-595.
[29] C. Boo, S. Hong, M. Elimelech, Relating Organic Fouling in Membrane Distillation to Intermolecular Adhesion Forces and Interfacial Surface Energies, Environmental science & technology, 52 (2018) 14198-14207.
[30] T. Horseman, C. Su, K.S. Christie, S. Lin, Highly Effective Scaling Mitigation in Membrane Distillation Using a Superhydrophobic Membrane with Gas Purging, Environmental Science & Technology Letters, (2019).

[31] Z. Wang, M. Elimelech, S. Lin, Environmental applications of interfacial materials with special wettability, Environmental science & technology, 50 (2016) 2132-2150.
[32] Z. Wang, J. Jin, D. Hou, S. Lin, Tailoring surface charge and wetting property for robust oil-fouling mitigation in membrane distillation, Journal of Membrane Science, 516 (2016) 113-122.
[33] Y.-X. Huang, Z. Wang, J. Jin, S. Lin, Novel Janus membrane for membrane distillation with simultaneous fouling and wetting resistance, Environmental science & technology, 51 (2017) 13304-13310.
[34] F. Zhao, Z. Ma, K. Xiao, C. Xiang, H. Wang, X. Huang, S. Liang, Hierarchically textured superhydrophobic polyvinylidene fluoride membrane fabricated via nanocasting for enhanced membrane distillation performance, Desalination, 443 (2018) 228-236.
[35] Z. Xiao, R. Zheng, Y. Liu, H. He, X. Yuan, Y. Ji, D. Li, H. Yin, Y. Zhang, X.-M. Li, T. He, Slippery for scaling resistance in membrane distillation: A novel porous micropillared superhydrophobic surface, Water Research, 155 (2019) 152-161.
[36] M. Xie, W. Luo, S.R. Gray, Surface pattern by nanoimprint for membrane fouling mitigation: Design, performance and mechanisms, Water research, 124 (2017) 238-243.
[37] C. Boo, J. Lee, M. Elimelech, Omniphobic polyvinylidene fluoride (PVDF) membrane for desalination of shale gas produced water by membrane distillation, Environmental science & technology, 50 (2016) 12275-12282.
[38] R. Zheng, Y. Chen, J. Wang, J. Song, X.-M. Li, T. He, Preparation of omniphobic PVDF membrane with hierarchical structure for treating saline oily wastewater using direct contact membrane distillation, Journal of membrane science, 555 (2018) 197-205.
[39] J. Lee, C. Boo, W.-H. Ryu, A.D. Taylor, M. Elimelech, Development of omniphobic desalination membranes using a charged electrospun nanofiber scaffold, ACS applied materials & interfaces, 8 (2016) 11154-11161.
[40] A. Razmjou, E. Arifin, G. Dong, J. Mansouri, V. Chen, Superhydrophobic modification of TiO2 nanocomposite PVDF membranes for applications in membrane distillation, Journal of membrane science, 415 (2012) 850-863.
[41] Y. Shao, M. Han, Y. Wang, G. Li, W. Xiao, X. Li, X. Wu, X. Ruan, X. Yan, G. He, Superhydrophobic polypropylene membrane with fabricated antifouling interface for vacuum membrane distillation treating high concentration sodium/magnesium saline water, Journal of membrane science, 579 (2019) 240-252.
[42] L.-H. Chen, A. Huang, Y.-R. Chen, C.-H. Chen, C.-C. Hsu, F.-Y. Tsai, K.-L. Tung, Omniphobic membranes for direct contact membrane distillation: effective deposition of zinc oxide nanoparticles, Desalination, 428 (2018) 255-263.
[43] C. Boo, J. Lee, M. Elimelech, Engineering surface energy and nanostructure of microporous films for expanded membrane distillation applications, Environmental science & technology, 50 (2016) 8112-8119.
[44] C. Lu, C. Su, H. Cao, X. Ma, F. Duan, J. Chang, Y. Li, F-POSS based omniphobic membrane for robust membrane distillation, Materials Letters, 228 (2018) 85-88.
[45] Y. Chen, M. Tian, X. Li, Y. Wang, A.K. An, J. Fang, T. He, Anti-wetting behavior of negatively charged superhydrophobic PVDF membranes in direct contact membrane distillation of emulsified wastewaters, Journal of membrane science, 535 (2017) 230-238.
[46] Y. Chul Woo, Y. Chen, L.D. Tijing, S. Phuntsho, T. He, J.-S. Choi, S.-H. Kim, H. Kyong Shon, CF4 plasma-modified omniphobic electrospun nanofiber membrane for produced water brine treatment by membrane distillation, Journal of Membrane Science, 529 (2017) 234-242.
[47] M. Tian, Y. Yin, C. Yang, B. Zhao, J. Song, J. Liu, X.-M. Li, T. He, CF4 plasma modified highly interconnective porous polysulfone membranes for direct contact membrane distillation (DCMD), Desalination, 369 (2015) 105-114.
[48] X. Wei, B. Zhao, X.-M. Li, Z. Wang, B.-Q. He, T. He, B. Jiang, CF4 plasma surface modification of asymmetric hydrophilic polyethersulfone membranes for direct contact membrane distillation, Journal of membrane science, 407 (2012) 164-175.
[49] C. Yang, X.-M. Li, J. Gilron, D.-f. Kong, Y. Yin, Y. Oren, C. Linder, T. He, CF4 plasma-modified superhydrophobic PVDF membranes for direct contact membrane distillation, Journal of membrane science, 456 (2014) 155-161.
[50] C. Yang, M. Tian, Y. Xie, X.-M. Li, B. Zhao, T. He, J. Liu, Effective evaporation of CF4 plasma modified PVDF membranes in direct contact membrane distillation, Journal of Membrane Science, 482 (2015) 25-32.

[51] Z. Wang, D. Hou, S. Lin, Composite membrane with underwater-oleophobic surface for anti-oil-fouling membrane distillation, Environmental science & technology, 50 (2016) 3866-3874.
[52] G. Zuo, R. Wang, Novel membrane surface modification to enhance anti-oil fouling property for membrane distillation application, Journal of membrane science, 447 (2013) 26-35.
[53] V. Karanikola, C. Boo, J. Rolf, M. Elimelech, Engineered slippery surface to mitigate gypsum scaling in membrane distillation for treatment of hypersaline industrial wastewaters, Environmental science & technology, 52 (2018) 14362-14370.
[54] E. Curcio, E. Fontananova, G. Di Profio, E. Drioli, Influence of the structural properties of poly (vinylidene fluoride) membranes on the heterogeneous nucleation rate of protein crystals, The Journal of Physical Chemistry B, 110 (2006) 12438-12445.
[55] E. Curcio, X. Ji, G. Di Profio, E. Fontananova, E. Drioli, Membrane distillation operated at high seawater concentration factors: Role of the membrane on CaCO3 scaling in presence of humic acid, Journal of Membrane Science, 346 (2010) 263-269.
[56] S. Meng, Y. Ye, J. Mansouri, V. Chen, Fouling and crystallisation behaviour of superhydrophobic nano-composite PVDF membranes in direct contact membrane distillation, Journal of membrane science, 463 (2014) 102-112.
[57] D.M. Warsinger, A. Servi, S. Van Belleghem, J. Gonzalez, J. Swaminathan, J. Kharraz, H.W. Chung, H.A. Arafat, K.K. Gleason, Combining air recharging and membrane superhydrophobicity for fouling prevention in membrane distillation, Journal of membrane science, 505 (2016) 241-252.
[58] Z. Xiao, Z. Li, H. Guo, Y. Liu, Y. Wang, H. Yin, X. Li, J. Song, L.D. Nghiem, T. He, Scaling mitigation in membrane distillation: From superhydrophobic to slippery, Desalination, 466 (2019) 36-43.
[59] C. Navier, Mémoire sur les lois du mouvement des fluides, Mémoires de l'Académie Royale des Sciences de l'Institut de France, 6 (1823) 389-440.
[60] J. Orfi, N. Loussif, P.A. Davies, Heat and mass transfer in membrane distillation used for desalination with slip flow, Desalination, 381 (2016) 135-142.
[61] Y.W. Park, N. Inagaki, Surface modification of poly(vinylidene fluoride) film by remote Ar, H2, and O2 plasmas, Polymer, 44 (2003) 1569-1575.
[62] X.-M. Li, T. He, M. Crego-Calama, D.N. Reinhoudt, Conversion of a Metastable Superhydrophobic Surface to an Ultraphobic Surface, Langmuir, 24 (2008) 8008-8012.
[63] M. Nosonovsky, B. Bhushan, Hierarchical roughness optimization for biomimetic superhydrophobic surfaces, Ultramicroscopy, 107 (2007) 969-979.
[64] T. Nishino, M. Meguro, K. Nakamae, M. Matsushita, Y. Ueda, The lowest surface free energy based on− CF3 alignment, Langmuir, 15 (1999) 4321-4323.
[65] T.A. Hoang, H.M. Ang, A.L. Rohl, Effects of temperature on the scaling of calcium sulphate in pipes, Powder Technology, 179 (2007) 31-37.
[66] D. Kashchiev, G.M.V. Rosmalen, Review: Nucleation in solutions revisited, Crystal Research & Technology, 38 (2010) 555-574.
[67] D.M. Warsinger, E.W. Tow, J. Swaminathan, J.H. Lienhard V, Theoretical framework for predicting inorganic fouling in membrane distillation and experimental validation with calcium sulfate, Journal of Membrane Science, 528 (2017) 381-390.
[68] C. Kunz, B. Lönnerdal, Human-milk proteins: analysis of casein and casein subunits by anion-exchange chromatography, gel electrophoresis, and specific staining methods, The American Journal of Clinical Nutrition, 51 (1990) 37-46.
[69] S. Srisurichan, R. Jiraratananon, A. Fane, Humic acid fouling in the membrane distillation process, Desalination, 174 (2005) 63-72.
[70] C.-H. Choi, C.-J. Kim, Large slip of aqueous liquid flow over a nanoengineered superhydrophobic surface, Physical

review letters, 96 (2006) 066001.
[71] H.S. Grewal, C. Il-Joo, O. Jae-Eung, Y. Eui-Sung, Effect of topography on the wetting of nanoscale patterns: experimental and modeling studies, Nanoscale, 6 (2014) 15321-15332.
[72] W. Bing-Bing, W. Hua-Ping, Z. Zheng, D. Chen-Chen, C. Guo-Zhong, Thermodynamic analysis of stable wetting states and wetting transition of micro/nanoscale structured surface, ACTA PHYSICA SINICA, 64 (2015).
[73] H. Wu, K. Zhu, B. Wu, J. Lou, Z. Zhang, G. Chai, Influence of structured sidewalls on the wetting states and superhydrophobic stability of surfaces with dual-scale roughness, Applied surface science, 382 (2016) 111-120.
[74] T. Pompe, S. Herminghaus, Three-phase contact line energetics from nanoscale liquid surface topographies, Physical review letters, 85 (2000) 1930.